Supplementary Material for

Spatial distribution of dissolved organic matter in ice and at air-ice interfaces

Subha Chakraborty[1,2] and Tara F. Kahan[1,2*]

1. Department of Chemistry, University of Saskatchewan, 110 Science Place, Saskatoon, SK 37N 5C9, Canada
2. Department of Chemistry, Syracuse University, 1-014 Center for Science and Technology, Syracuse, NY 13244, USA

*Author to whom correspondence should be addressed: tara.kahan@usask.ca, Ph: +1 (306) 966-1168.

Section S1: Analysis procedure for deconvolution of contributions from liquid water and ice in frozen solution spectra

When solutes are present in frozen aqueous solutions, solute-induced melting occurs. This can result in distortion of the Raman spectrum of the O–H stretching region of pure ice, since the acquired spectrum consists of a spectral fraction from ice and from liquid water. The spectrum of bulk deionized (DI) water (at room temperature) and the surface of DI water ice (at –25 °C), are shown in the main article in FIG. 1(b) and (c) respectively. It is expected that at –25 °C, the surface of DI water ice does not contain any detectable amount of liquid water or disorder in the surficial hydrogen bonds, and hence the spectrum can be considered as a reference spectrum of pure ice. At any higher temperature, *T*, the acquired mixed spectrum, *IW* (*k*, *T*), can be written as a linear superposition of the spectrum of pure ice, *I*(*k*, –25 °C), and that of super-cooled water, *W*(*k*, *T*), as

$$IW = a\left[\left(1 - x_{\mathrm{W}}\right)I + x_{\mathrm{W}}W\right] \tag{s1}$$

where k is the wavenumber, x_{W} is a fraction we define as spectral liquid contribution (that determines how much of the acquired spectrum is contributed by super-cooled water), and a is a proportionality constant that takes into account the differences in the integration times used for measuring *IW* and the reference spectra. The reference spectra, *I* and *W*, are both normalized to their corresponding maximum intensities. A value of $x_{\mathrm{W}} = 0$ means there is no water in the observed spectrum and a value of 1 means there is no ice in the spectrum. Absolute values of x_{W} other than 0 and 1 do not hold any significance as such; however, a comparison among x_{W} values indicate a relative increase or decrease of liquidity of the ice surface as temperature or concentration of the solute is changed.

FIG. S1 shows spectra of liquid water at temperatures ranging from 25 °C to −14 °C. Freezing did not occur until −15 °C due to a lack of nucleation sites. In our experimental setup, the liquid water spectrum could not be acquired at temperatures below −14 °C. Hence for any temperature of ice surface lower than −14 °C, the spectrum of the super-cooled water, if any, is approximated by the spectrum at −14 °C.

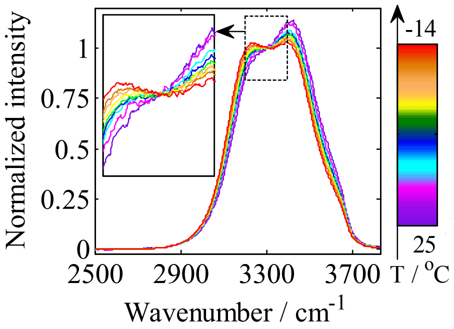

FIG. S1: Raman spectra of DI water as the temperature, *T*, is decreased from 25 °C to −14 °C. Each spectrum is normalized by the counts at 3300 cm^{-1} (isosbestic point) for visual consistency. The colours of the spectra correspond to the temperatures in the colour bar and the arrow describes the direction of temperature change. The section in the dashed rectangle, centred at 3300 cm^{-1}, is magnified in the inset to show the relative changes in the spectra with temperature.

FIG. S2 shows examples of using Eqn. (s1) to extract x_W from the exemplary spectrum of the three types of solutes studied in the main article in FIG. 1(c). For humic acid, the background fluorescence emission in the range 2502 – 2800 cm^{-1} and in the range 3800 – 3830 cm^{-1} is combined and a 3rd order polynomial fitting is used to interpolate the spectrum between 2800 and 3800 cm^{-1}. Once the background is achieved, it is subtracted from the acquired spectrum to extract the spectrum IW that can be written as Eqn. (s1). Similarly, for sodium dodecyl sulphate (SDS) and citric acid, the background is extracted from the region 2502 – 2700 cm^{-1}, and in the range 3800 – 3830 cm^{-1}. The background-subtracted spectra are shown in FIG. S2(a) through (c). A comparison with the spectrum of DI water ice in each panel shows the difference in the O–H stretching region of the spectrum due to inclusion of the solute. Next, Pearson correlation, ρ, is evaluated between this subtracted spectrum and a hypothetical spectrum given by Eqn. (s1) by varying x_W between 0 and 1. In FIG. S2(d) through (f), the maps of ρ with x_W and T are shown for the three spectra. In each case, global maxima in the values of ρ can be obtained, indicating the best-fit results. The corresponding values of x_W and T are shown as a marker in each map. The fitted spectra are reproduced in blue in FIG. S2(a) through (c) to compare with the acquired spectrum. In all cases, the corresponding maximum values of ρ between the fitted spectrum and the acquired spectrum (after background subtraction) is greater than 0.995, indicating very high goodness of fit. It is interesting to note that in all cases, the best correlation is obtained when the spectrum is compared taking the spectrum of super-cooled water below −10 ° (true temperature of spectrum acquisition = −15 °C), indicating that the distortion in the O–H stretching region from that of pure DI water by inclusion of the solutes is, perhaps, representable by super-cooled water. However, there is consistent deviation between the acquired spectrum and the fitted spectrum in the region 3500 – 3700 cm^{-1}. It is also noteworthy from FIG. S2(d) through (f) that if, instead of finding the global maxima of ρ with both x_W and T, the maxima was evaluated only by comparing the spectrum of room temperature water, the corresponding x_W do not change by more than 10% for SDS and humic acid samples. For citric acid, the change is about 25%, which means that the values of x_W would be correct within 25% if the room temperature samples were used for the spectral decomposition.

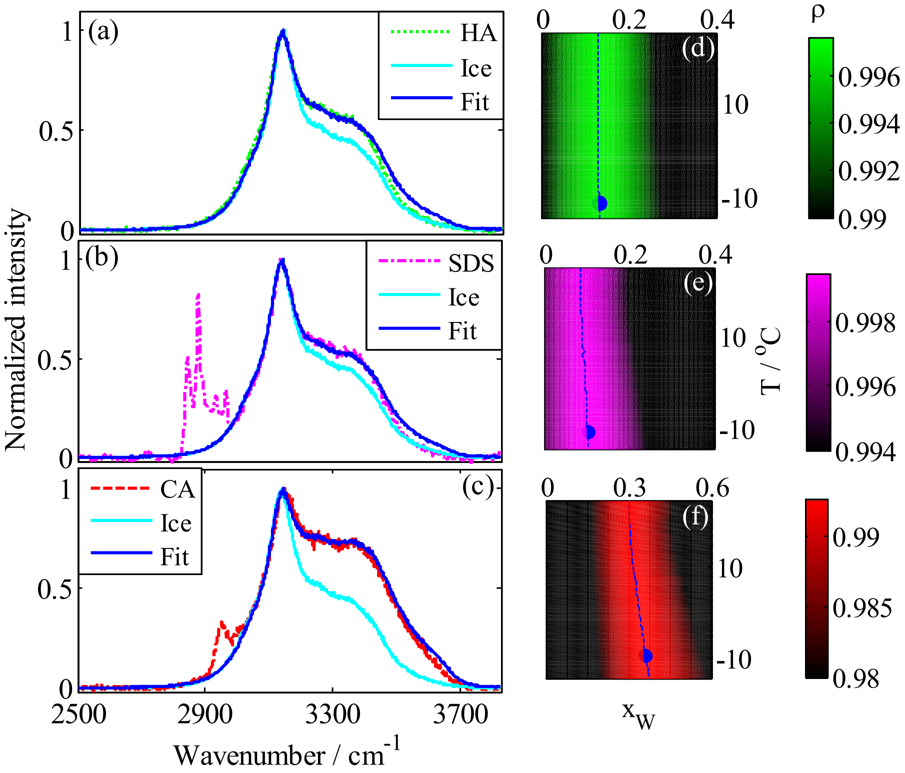

FIG. S2: Exaple of deconvolutions of frozen solution spectra into pure ice and unfrozen solution for (a) HA, (b) SDS, and (c) CA solutions. The same spectra from FIG. 1(c) in the main article are used. In each case, the background subtraction is performed to show the O-H Raman stretch for the analysis based on Eqn. (s1). The pure ice spectrum at −25 °C is also shown in all figures. The Pearson correlation, ρ, is evaluated by varying x_W and T to obtain the global maximum. For each T, the corresponding spectrum of super-cooled water from FIG. S1 is used. The map of ρ with x_W and T are shown in (d) through (f) for the three samples. The bold blue marker shows the global maximum and the blue dashed line represents the maximum of ρ at each temperature, i.e., the value of x_W at each T that corresponds to the maximum along the correponding horizontal direction in the maps. The fitted spectra correponding to these maxima are reproduced in FIG. (a) – (c).

The consistency of this method of analyzing x_W has been verified for pure DI water ice. At different sub-freezing temperatures, the extracted values of x_W from a location at the DI water ice surface as a function of laser exposure time are shown in FIG. S3 for up to 100 sec. The moving average values of x_W are shown in black dashed lines. At all times, the maximum correlation value, ρ, was obtained to be above 0.995, similar to the correlations obtained from the cases of frozen solutions. There is minimal change in the value of x_W over time, indicating that the laser exposure even up to 100 sec at power levels used in the mapping experiments in the main article does not melt the surface of ice to an extent that would lead to an increasing value of x_W. For higher temperatures, such as −2 °C, higher mean values of x_W are obtained, while at −25 °C, the mean value was 0.001. Since we expect hardly any water to be at ice surface at this temperature, the non-zero value of x_W thus sets a lower limit of detection for any liquid water on frozen surfaces. Over repeated measurements, we observed that the random error in the value of x_W at −25 °C can be as high as 0.003, perhaps due to random noise of the CCD detector (less than 2% of the peak at integration times greater than 0.5 sec). Therefore, a safe cut-off for any reliable measurement of x_W from frozen solutions is set to 0.006, such that any value of $x_W \geq 0.006$ from a position on the surface of the frozen solution indicates the presence of liquid at that location and any value of $x_W < 0.006$ indicates the absence of liquid. It can be noted that inclusion of x_W in the analysis ensures that the linear superposition of the reference spetra I and W indeed yield a value of ρ higher than 0.995 in all cases. For example, correlation measurement without considering x_W (i.e. $x_W = 0$) between I acquired at −25 °C and −2 °C leads to a value less than 0.99 over an entire DI water surface, but with x_W as a fitting parameter to maximize correlation leads to a value consistently higher than 0.995. The best-fit results of x_W determines the distortion in the spectrum, having a mean value of 0.008 over the entire surface. With decreasing temperature, we observe a gradual decrease in the mean value with a mean value of 0.001 at −15 °C. For samples containing solutes, we always get a correlation higher than 0.995 after the best-fit is applied, and the corresponding values of x_W are significantly higher than those observed in frozen DI water. Hence, setting a threshold of x_W = 0.006 indeed represents a conservative cut-off in measurability of liquid solutions on the ice surface and any value higher than 0.006 is truly due to distortion in the spectrum, and not an artefact.

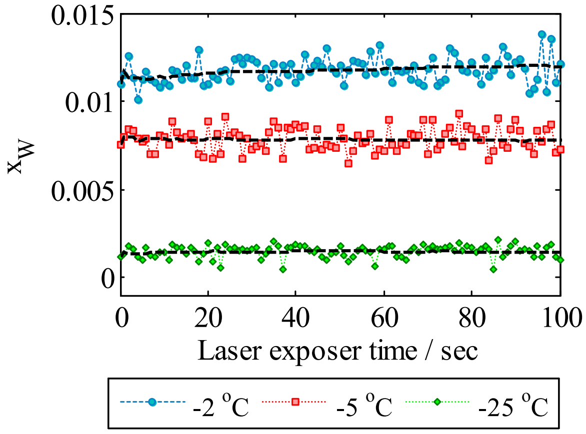

FIG. S3: Consistency measurement of spectral liquid contribution, x_W, measured at a single spot on the surface of pure ice at different temperatures for 100 sec. of continuous laser illumination. The constancy of the measurements is described by the moving average values shown in dashed black lines.

Section S2: Solute concentration calibration curves in the liquid phase and determination of limits of detection

Figure S4 shows plots of normalized intensities of the liquid solutions of the three different solutes as a function of their bulk concentrations. In all cases, intensity refers to fluorescence background for humic acid and the peak of the C–H stretch in SDS and citric acid shown in FIG. 1(b) of main article, normalized to maximum intensity of the spectra, typically at 3135 cm^{-1}.

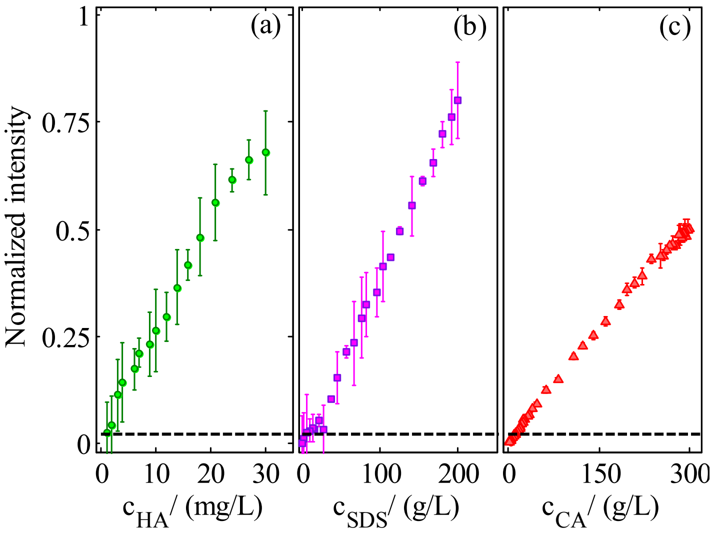

FIG. S4: Normalized intensity as a function of solute concentration for (a) HA, (b) SDS, and (c) CA. The black dashed line is the upper limit of dark background (0.02) that is obtained from the spectrum of pure water, setting the lower limit of detection (LOD) of concentration from these plots. For HA, SDS and CA, the LODs are respectively 1 mg/L (HA), 10 g/L (SDS), and 20 g/L (CA).

Section S3: Analysis procedure for identifying solutes in spectra

After background subtraction as shown in FIG. S1, the intensity of the peak in the C–H stretching region (2800 – 3100 cm^{-1}) is normalized to the peak of the O-H stretching region (~3135 cm^{-1}) for SDS and citric acid frozen solutions. The surface maps of these normalized intensities are shown in FIG. 2 in the main article. For humic acid, the average fluorescence background is normalized to the peak of the O–H stretching region. The calculated ratio is compared with the corresponding ratio for pure ice at −25 °C in order to evaluate whether solute is present at that location. In order to determine a cut-off value, we add a constant value of 13 counts to the true intensity at the position of the C–H stretching peak in the Raman spectrum of pure ice to set a conservative limit of detection. The number 13 is determined from the statistical noise-floor of the measurement system in a method described below.

Figure S5 shows the dark noise distribution of the charge coupled device (CCD) detector at 0.25 sec integration time. The signal counts are segmented into 41 intervals and the number of pixels recording a count within each interval is obtained and plotted against the centre of each interval. The error bar on the experimental data is obtained by recording 1000 spectra and finding the standard deviation at each interval. The figure shows that the dark noise distribution of the CCD can be nicely fitted to a Gaussian noise distribution with a standard deviation of 3.8 ± 0.1 counts over a mean of about 1 dark count. Repeated measurements between 0.1 sec and 10 sec integration times show nearly identical results, with an overall estimated standard deviation of noise distribution $\sigma_{CCD} = 3.7 \pm 0.2$ over a mean dark count $\mu_{CCD} = 1.1 \pm 0.3$. The constancy of the mean dark count over the wide range of integration time is due to internal dark calibration of the CCD. It can be shown from the properties of Gaussian noise that at least 1014 out of the 1015 pixels of the CCD are expected to produce a random noise within $3.3\sigma_{CCD} \approx \pm 12$ about the mean. Therefore, a conservative upper limit of the dark count at all pixels can be written as $|\mu_{CCD} + 3.3\sigma_{CCD}| = 13$ counts for all pixels. Since this is the upper limit of noise for all the pixels where the normalized intensity is evaluated and compared to the corresponding normalized intensity from pure ice, we can add this cut-off to the counts of pure ice before normalization and comparing, such that the probability that solute would be detected as an artefact from noise is minimal.

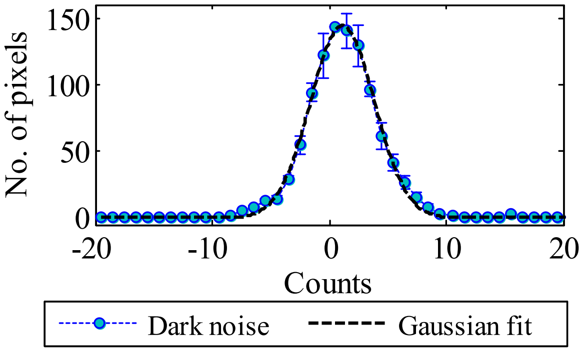

FIG. S5: Dark noise distribution of the CCD at 0.25 sec integration time. Dark counts are recorded and segmented into 41 intervals between −20 and 20. The number of pixels recording dark count in each interval is plotted against the centre of each interval. The error bar on the experimental data is obtained by recording 1000 spectra and finding the standard deviation of the number of pixels.

Section S4: Surface maps of frozen solutions of humic acid, SDS, and citric acid at −5 °C, −15 °C, and −25 °C

The surface maps shown in FIG. S6 through S8 are to complement the surface maps shown in FIG. 2 of the main article for the same samples at two other temperatures, one 10 °C warmer than the temperature (−15 °C) shown in the main article and another 10 °C colder. FIG. S9 shows temperature dependences of liquid surface coverage averaged over the entire scanned area.

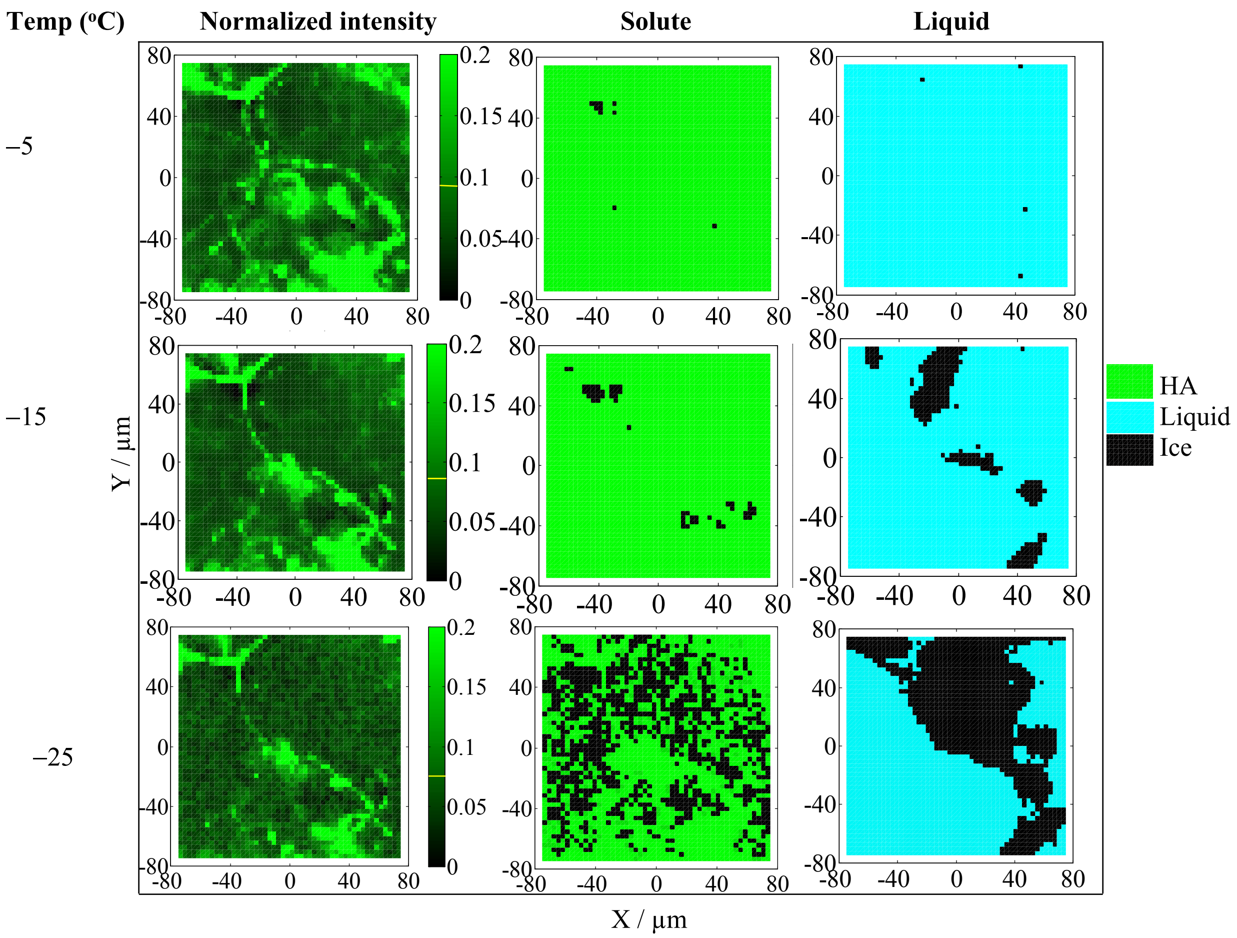

FIG. S6: Surface maps of intensities normalized to 3135 cm^{-1} (left column), solute surface coverage (middle column), and surface coverage of liquid water (right column) for humic acid, with pre-frozen concentration of 3 mg/L, from the same sample shown in FIG. 2 of the main article at three temperatures. *X* and *Y* represent two orthogonal directions on the surface.

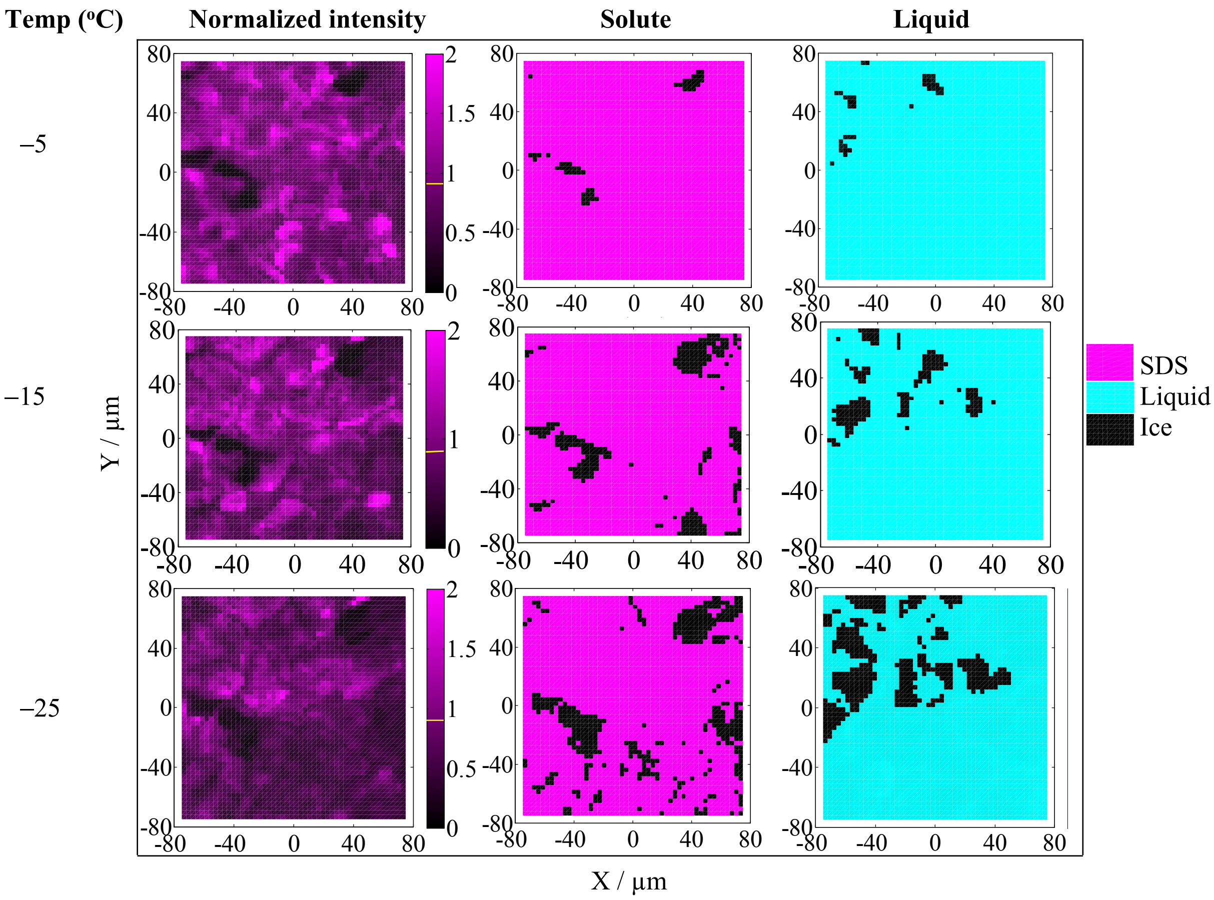

FIG. S7: Surface maps of intensities normalized to 3135 cm^{-1} (left column), solute surface coverage (middle column), and surface coverage of liquid water (right column) for SDS, with with pre-frozen concentration of 1 g/L from the same sample shown in FIG. 2 of the main article at three temperatures. *X* and *Y* represent two orthogonal directions on the surface.

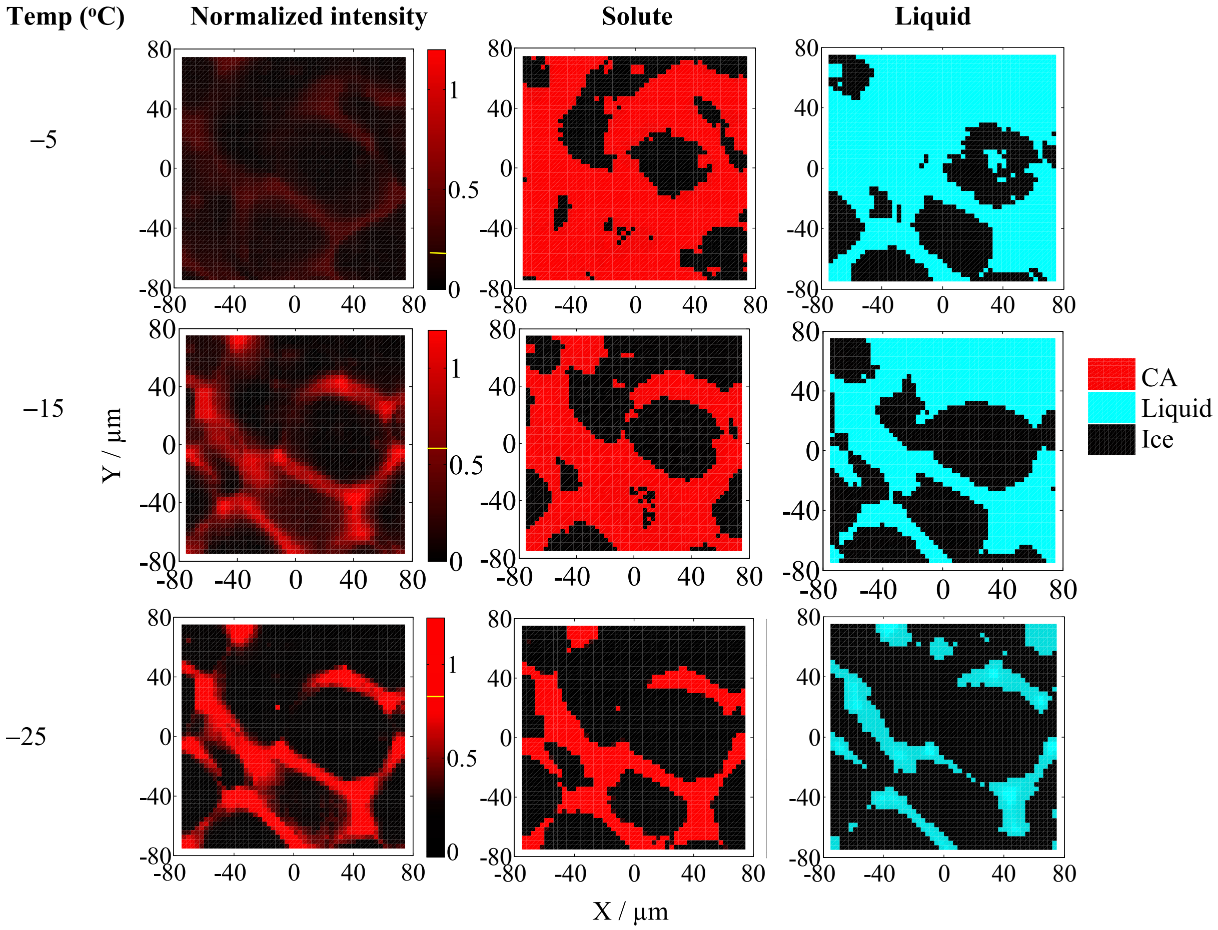

FIG. S8: Surface maps of intensities normalized to 3135 cm^{-1} (left column), solute surface coverage (middle column), and surface coverage of liquid water (right column) for citric acid solutions with pre-frozen concentrations of 60 g/L from the same sample shown in FIG. 2 of the main article at three temperatures. *X* and *Y* represent two orthogonal directions on the surface.

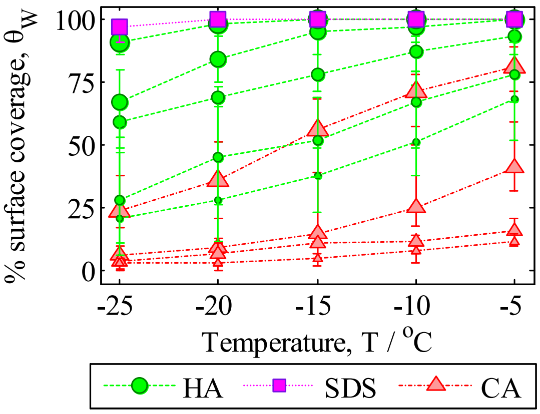

FIG. S9: Plot of liquid surface coverage from all frozen samples as a function of temperature. Increasing marker size indicates increasing pre-frozen concentrations: 0.003 mg/L, 0.03 mg/L, 0.3 mg/L, 3 mg/L and 30 mg/L (HA); 1 g/L and 10 g/L (SDS); and 0.06 g/L, 0.6 g/L, 6 g/L and 60 g/L (CA).